[redacted] CONFIDENTIAL

Copy 227
RM E56L03

NACA

RESEARCH MEMORANDUM

Log # 7580

MAR 1 1 1957

OBSERVATION OF LAMINAR FLOW ON AN AIR-LAUNCHED 15° CONE-CYLINDER AT LOCAL REYNOLDS NUMBERS TO 50×10^6 AT PEAK MACH NUMBER OF 6.75

By Leonard Rabb and Milan J. Krasnican

Lewis Flight Propulsion Laboratory
Cleveland, Ohio

NATIONAL ADVISORY COMMITTEE
FOR AERONAUTICS

WASHINGTON

March 4, 1957

[redacted]

[redacted]

NACA RM E56L03

[redacted]

NATIONAL ADVISORY COMMITTEE FOR AERONAUTICS

RESEARCH MEMORANDUM

OBSERVATION OF LAMINAR FLOW ON AN AIR-LAUNCHED 15° CONE-CYLINDER AT LOCAL REYNOLDS NUMBERS TO 50×10^6 AT PEAK MACH NUMBER OF 6.75

By Leonard Rabb and Milan J. Krasnican

SUMMARY

A free-flight test vehicle was flown to obtain boundary-layer-transition and heat-transfer data. The model was a 15°-included-angle cone-cylinder with a 10° conically flared afterbody. The nose tip was hemispherically shaped with a diameter 15 percent of the cylinder diameter. The model was launched 27° downward from a carrier airplane at an altitude of 43,360 feet and reached a maximum Mach number of 6.75 at 28,100 feet. Laminar flow was indicated on the forward (highly polished) portion of the model to Reynolds numbers of 50×10^6. Turbulent flow was indicated for the aft (unpolished) measuring stations.

INTRODUCTION

Designers of hypersonic aircraft and missiles have been increasingly aware of the problems associated with aerodynamic heating. Of special interest is the problem of maintaining a laminar boundary layer over large surface areas. The advantages of long runs of laminar boundary layers are well understood. However, the factors affecting boundary-layer transition are not so clearly defined. Additional experimental data at hypersonic speeds and high stagnation temperatures are needed.

The NACA Lewis laboratory is currently investigating the many problems associated with aerodynamic heating. Among the research tools being utilized is the technique of air-launched free-flight test-bodies. The test bodies are accelerated to hypersonic speeds by booster rockets. Both single-stage and multistage rocket configurations have been flown. The results of previous flights are presented in references 1 to 4. The present test was made to obtain additional data at higher Reynolds numbers.

[redacted]

[redacted]

APPARATUS AND PROCEDURE

The test body, shown in figure 1, is identical to the configuration discussed in reference 4. The model was aerodynamically stabilized by a flared section or "skirt" at the rear and small wedge-shaped fins attached to the skirt. These fins provided additional stability at the point of booster separation. The tip of the 15°-included-angle cone was a hemisphere with a diameter of 7/8 inch, and the cylindrical afterbody diameter was 6 inches.

The test body was assembled in two pieces, with the skin juncture or parting line located at station 32.88. The skin was nominally 1/16-inch-thick Inconel along the cone and 1/32-inch-thick Inconel beyond the cone-cylinder shoulder (station 20.03). The actual skin thicknesses at each of the instrumented stations and the wetted surface distance to each station are presented in figure 1. In order to increase the emissivity and thus reduce the anticipated higher skin temperatures, the rear surface of the body (aft of the parting line) was chemically blackened. The skin forward of the parting line was highly polished by a commercial diamond paste to a surface finish of the order of 2 microinches. The highly polished nose section is shown in figure 2. The sustainer rocket (T-55) occupied the volume aft of the parting line.

All data were transmitted to ground receiving stations by means of the radio-telemeter assembly located in the volume forward of the parting line. The small fins near the parting line (fig. 1) served as the transmitting antenna. Temperature measurements were telemetered on one channel but were switched to record a total of 12 measurements at intervals of about 0.2 second. All of the thermocouples were Chromel-Alumel and were in line except at stations 19.40, 60.81, and 67.56 (fig. 1). The remaining data were recorded continuously from a static-pressure tap and two axial accelerometers. The type and ranges of the instrumentation are as follows:

Quantity	Range
Axial acceleration, g's	0 to 90
Axial acceleration, g's	0 to -25
Static pressure, lb/sq ft abs	0 to 2160
Skin temperature (thermocouple), °R	400 to 1700

Figure 3 shows the booster assembly, which consisted of a thin-wall (1/16-in.) aluminum tube with cruciform aluminum fins mounted at the rear. The fins were 1/4 inch thick, with the leading edges tapered and rounded to a 1/16-inch radius. The booster rocket (T-40), which was housed within the aluminum shell, was maintained at a temperature of 100° F before firing by wrapping it with an electric blanket. The sustainer rocket was not heated before launching.

The booster assembly was rigidly connected to the final stage with a coupling that was destroyed by the ignition of the final-stage rocket. The coupling was developed by the NACA Langley laboratory and is described in reference 5. Table I gives some physical information on the two-stage test body. Table II presents data on the two rockets used.

The test body was carried aloft by the F2H-2B airplane shown in figure 4. The model was launched 27° downward at an altitude of 43,360 feet. Time-delay squibs were used to ignite both rockets, and the test body was tracked by ground radar and phototheodolite equipment.

The calculation procedure used in these flight tests is detailed in references 2 and 4. The free-stream velocity was determined from radar measurements and by integrating the acceleration data. The altitude was obtained from radar measurements and the static-pressure measurement at station 29.88. The variation of ambient pressure and temperature with altitude was determined from a radiosonde survey made immediately following the flight.

The local flow conditions for this test body were computed for two cases. Case I assumed that the nose of the model was sharply pointed and that the flow along the cone-cylinder was represented by the calculations of references 6 and 7 as applied to the specific configuration of this test. The flow properties of case I are designated "sharp-tip" conditions.

The local flow properties computed for case II are designated "blunt-tip" conditions. Case II attempts to account for tip bluntness effects by using the method of reference 8. This assumes that the surface static pressure along the body, downstream of the blunted tip, is the same as for a sharply pointed body. By assuming a normal-shock total-pressure loss at the nose, the air in a small annular area about the body is at a much lower Mach number than that of the sharply pointed body. This layer of low Mach number air blankets the boundary layer. The amount of tip blunting, of course, determines the length of boundary layer that may be affected. Approximate calculations based on reference 8 indicate that the tip bluntness of the present test vehicle was insufficient to completely cover the boundary layer over the entire body.

[redacted]

RESULTS AND DISCUSSION

The time histories of the axial acceleration (exclusive of gravity) and the free-stream velocity are presented in figure 5. The velocity at release was 754 feet per second. At 5.34 seconds, the booster rocket fired and accelerated the model to 4106 feet per second. The sustainer rocket fired at 11.44 seconds and accelerated the model to a peak velocity of 6874 feet per second at 13.0 seconds. A maximum acceleration of 63.56 g's was recorded at 12.6 seconds. The telemeter radio transmission stopped shortly thereafter at 13.23 seconds. Accelerometer measurements (not shown in fig. 5) indicated that the model tumbled just before the end of the record.

Free-Stream Conditions

The time histories of the following free-stream conditions are presented in figure 6: (a) altitude, (b) static pressure, (c) static temperature, (d) total temperature and adiabatic wall temperature, (e) Reynolds number per foot, and (f) Mach number. The free-stream static pressure of figure 6(b) was obtained from radiosonde readings. The measured static pressure at station 29.88 is also shown in figure 6(b) and varies a maximum of 5 percent from radiosonde data when corrected by the method of reference 7. The maximum total temperature of 3864° R (fig. 6(d)) occurred at 13.0 seconds. The adiabatic wall temperature (fig. 6(d)) was based on the theoretical laminar recovery factor (square root of Prandtl number). The free-stream Reynolds number per foot of figure 6(e) was a maximum at 13.2 seconds, because the increasing density offset the decrease in velocity between 13.0 and 13.2 seconds. The maximum free-stream Reynolds number per foot of 20.8×10^6 gave a maximum free-stream Reynolds number of 125×10^6 based on a model length of 6 feet. The free-stream Mach number (fig. 6(f)) reached a maximum of 6.75 at 13.0 seconds at an altitude of 28,100 feet (fig. 6(a)).

Conditions at Outer Edge of Boundary Layer

Time histories of the Mach number and Reynolds number per foot just outside the boundary layer at each of the temperature measuring stations are shown in figures 7 and 8 for cases I and II. Correcting for tip bluntness reduced the peak Mach number on the cone from 5.84 (fig. 7(a)) to 2.75 (fig. 7(b)). The maximum Mach number based on sharp-tip properties was 7.03 at station 21.65. This is slightly greater than free-stream Mach number because of the local flow expansion around the cone-cylinder junction.

The local Reynolds number per foot based on sharp-tip conditions (fig. 8(a)) reached a peak at 13.2 seconds. The local per foot values

of Reynolds numbers were higher on the cone and the flared afterbody than on the cylinder. Peak Reynolds number per foot of 33.7×10^6 was calculated for station 67.56. This gave a Reynolds number of 97×10^6 based on a length of 2.89 feet. The maximum cone Reynolds number was 50.2×10^6 at station 19.40.

The values of Reynolds number per foot based on blunt-tip conditions are shown against time in figure 8(b). Reynolds number per foot on the cone and flare remained nearly constant with increasing time, but cylinder values fell approximately 30 percent.

Temperatures and Heat-Transfer Coefficients

The measured skin temperatures are shown in figure 9. The maximum skin temperature of approximately 1820° R was measured at station 67.56 at 13.2 seconds (fig. 9(d)). The rate of rise of skin temperature at this station was 1180° R per second at the time of model failure (13.2 sec). Such a high temperature and rate of temperature rise on the flared skirt may have caused the structure to fail and could have initiated the tumbling action mentioned earlier. The skin temperatures forward of station 31.72 were relatively cool compared with those at stations 60.81 and 67.56.

The telemeter records showed abrupt discontinuities in the skin temperature measurement of 10° to 40° R at times of booster and sustainer rocket ignition. These discontinuities did not noticeably alter the slope of the traces of temperature against time and were treated as zero shifts in the temperature analysis. In addition, the measured skin temperatures (except for station 67.56) did not cover the full temperature range of the thermocouples. Because of these factors, the heat-transfer coefficients (fig. 10), which were derived from the skin-temperature measurements, may have large percentage errors. However, the data are accurate enough to distinguish between laminar and turbulent boundary layers.

The temperature measurements for two stations located nearly 180° apart are shown in figure 9(b). The data showed excellent agreement between both stations, which indicated similar boundary-layer development on both sides of the test model.

The heat-transfer coefficients are shown in figure 10 in dimensionless form as Stanton numbers. The data are compared with theoretical laminar and turbulent values from references 9 to 13. The theoretical Stanton numbers of figure 10 are based on local blunt-tip flow conditions. Reference 8 shows that the theoretical laminar heat-transfer rates are relatively unchanged when based on either sharp- or blunt-tip flow conditions. The same does not hold true for the turbulent boundary

layer. Calculations based on the Stanton numbers of reference 12 indicate that the theoretical turbulent heat-transfer rate may be reduced as much as 40 percent if blunt-tip local flow conditions apply.

The data of figure 10 indicate that laminar flow exists during the flight at all stations forward of and including station 31.72. This is in agreement with the data reported in reference 4 at somewhat lower Reynolds numbers. The maximum Reynolds numbers (based on the wetted distance from the stagnation point) on the cone and at station 31.72 were 50.2 and 49×10^6, respectively, during the present flight.

Stations 60.81 and 67.56 indicate a turbulent boundary layer during the flight. The theoretical Stanton numbers for both of these stations (fig. 10(d)) are based on local cone flow with blunt-tip conditions. The reference length for the Reynolds number at these stations has arbitrarily been taken from the parting line at station 32.88, because the flow was known to be laminar ahead of this station. The theoretical Stanton numbers at station 60.81 overestimate the heat-transfer rate throughout the time history. At station 67.56 the data are again less than turbulent theory until about 12.2 seconds. The data rise after 12.2 seconds and exceed the theory by a considerable amount. No explanation for this sudden increase in the Stanton number is now known. However, to illustrate the magnitude of the heat-transfer rate, the measured heating rate is compared in figure 11 with several theoretical estimates.

The theoretical heating rates shown in figure 11 are for both wedge and cone local flow conditions with sharp and blunt tips and for two choices of the Reynolds number reference length. These lengths are 5.04 inches (distance from cylinder-flare junction to station 67.56) and 34.68 inches (distance from parting line to station 67.56). It is obvious that the blunt-tip theoretical values of heating rate do not agree with the measured heating rate beyond 12.2 seconds. Sharp-tip conditions show better agreement, but it is not clear which of the various local flow conditions are valid and why. The data of reference 14 indicate that the heat-transfer rate on the flare may be predicted by choosing a reference length for the Reynolds number from the flare-cylinder junction. However, no definite conclusion can be derived from the present data. Also, it is not clear why blunt-tip conditions predict the heating rate reasonably well up to 12.2 seconds and sharp-tip conditions are better thereafter. It is evident that further data on flared afterbodies are needed before heat-transfer rates can be predicted with confidence.

The maximum heating rate measured was 735,000 Btu per square foot per hour for station 67.56 at 13.2 seconds. During this time interval (12.2 to 13.2 sec), the free-stream Mach number varied from approximately 5.0 to 6.7.

Boundary-Layer Stability Conditions

Lees (ref. 15), Dunn and Lin (ref. 16), and Van Driest (ref. 17) have shown that a laminar boundary layer may be stable at very large Reynolds numbers, provided the boundary layer is cooled sufficiently and the local Mach number falls within certain limits. The critical theoretical ratios of wall to local stream temperature from reference 16 are presented in figure 12 as a solid line. The symbols represent the data of this flight. Also shown in figure 12 are local Reynolds numbers. The data are shown for both sharp- and blunt-tip conditions.

Each station on the cone had laminar flow and was well within the stability curve of reference 16. For example, the data of station 19.32 (fig. 12(a)), which was typical of all the stations on the cone, were well within the stability limits for both sharp- and blunt-tip conditions. At peak Mach number, the sharp-tip Reynolds number was reduced from 49×10^6 to a blunt-tip value of 6×10^6. Reductions in ratio of wall to local stream temperature and local Mach number were from 1.00 to 0.32 and 5.85 to 2.75, respectively. The sharp-tip conditions for the stations on the cylinder forward of the parting line (figs. 12(b) to (d)) were outside the theoretical stability limit near the peak Mach numbers. However, the local conditions corrected for bluntness were well within the stability loop. The heat-transfer coefficients at these stations indicated laminar flow; thus, it appears that blunt-tip conditions were governing the local boundary-layer development.

Turbulent boundary layers were indicated for stations 60.81 and 67.56 in figure 10(d). However, the ratio of blunt-tip wall to local stream temperature (figs. 12(e) and (f)) were well within the stability limits of reference 16. The surface discontinuity at the parting line and the telemetering antenna (which was forward of these stations) may have triggered the boundary layer. Also, the skin aft of the parting line was not polished. The increased roughness could have promoted transition, even though the local blunt-tip temperature ratios were within the theoretically stable limits. Another possible explanation might be that the full effect of blunting the tip was not realized this far back on the model. Approximate calculations based on reference 8 indicated that a larger tip bluntness would be required to blanket the local boundary layer with low Mach number air at stations 60.81 and 67.56. Sharp-tip conditions could then be controlling the boundary layer. For this case the turbulent boundary layer may have been caused by either the high local Reynolds number or the surface roughness.

The ratio of wall to local stream temperature is plotted against blunt-tip Reynolds number in figure 13. The solid line represents a summary curve of transition data from references 3 and 18. Data are shown for two stations (9.84 and 31.72) from the present test flight

and two similar stations from reference 4. A comparison of stations 9.84 and 31.72 with the corresponding stations of reference 4 shows a 60-percent increase in local blunt-tip Reynolds number at the same ratio of wall to local stream temperature. The local sharp-tip Reynolds number was as high as 49×10^6 without evidence of transition for the present test. The blunt-tip flow conditions, however, were well below the values for which transition was obtained with sharp-tip models in references 3 and 18. Consequently, with the effect of blunting considered, no transition would be expected in the present tests.

SUMMARY OF RESULTS

A highly polished 15°-included-angle cone-cylinder with a hemispherical tip diameter 15 percent of the cylinder diameter was flown to obtain boundary-layer-transition data. The following results were obtained:

1. A maximum free-stream Mach number of 6.75 was attained at 28,100 feet following a 27° downward launching from an F2H-2B airplane. Peak sharp-tip Reynolds numbers on the cone and the flared afterbody were 50.2×10^6 and 97×10^6, respectively.

2. Laminar flow was observed on the highly polished cone-cylinder at the maximum sharp-tip Reynolds number of 50.2×10^6. The local blunt-tip ratios of wall to local stream temperature were well within the theoretical stability limits.

3. The maximum observed skin temperature was 1820° R, and the maximum observed heating rate was 735,000 Btu per square foot per hour. These values occurred on the flared afterbody.

4. Turbulent flow was observed on the aft part of the cylinder and on the flared surface of the model for local blunt-tip conditions well within the theoretically stable limits. However, surface roughness and a discontinuity at the missile parting line may have induced transition. Also, calculations indicate that the hemispherical tip may not have been large enough to produce the required layer of low Mach number air for blunt-tip conditions to apply fully at the rear of the missile.

5. The usual assumptions used to calculate the heat-transfer rates on the flared afterbody underestimated the heating rate during the last second of the flight history. During this time interval, the free-stream Mach number varied from approximately 5.0 to 6.7.

Lewis Flight Propulsion Laboratory
National Advisory Committee for Aeronautics
Cleveland, Ohio, December 5, 1956

REFERENCES

1. Messing, Wesley, E., Rabb, Leonard, and Disher, John H.: Preliminary Drag and Heat-Transfer Data Obtained from Air-Launched Cone-Cylinder Test Vehicle over Mach Number Range from 1.5 to 5.18. NACA RM E53I04, 1953.

2. Rabb, Leonard, and Simpkinson, Scott H.: Free-Flight Heat-Transfer Measurements on Two 20°-Cone-Cylinders at Mach Numbers from 1.3 to 4.9. NACA RM E55F27, 1955.

3. Rabb, Leonard, and Disher, John H.: Boundary-Layer Transition at High Reynolds Numbers as Obtained in Flight of a 20° Cone-Cylinder with Wall to Local Stream Temperature Ratios Near 1.0. NACA RM E55I15, 1955.

4. Disher, John H., and Rabb, Leonard: Observation of Laminar Flow on a Blunted 15° Cone-Cylinder in Free Flight at High Reynolds Numbers and Free-Stream Mach Numbers to 8.17. NACA RM E56G23, 1956.

5. Thibodaux, Joseph G., Jr.: A Brief Summary of Experience in Boosting Aerodynamic Research Models. NACA RM L56E28, 1956.

6. The Staff of the Computing Section Center of Analysis: Tables of Supersonic Flow Around Cones. Tech. Rep. No. 1, M.I.T., 1947. (Contract NOrd 9169.)

7. Clippinger, R. F., Giese, J. H., and Carter, W. C.: Tables of Supersonic Flows About Cone Cylinders. Pt. I: Surface Data. Rep. No. 729, Ballistic Res. Labs., Aberdeen Proving Ground (Md.), July 1950. (Proj. TB3-0108H of Res. and Dev. Div., Ord. Dept.)

8. Moeckel, W. E.: Some Effects of Bluntness on Boundary-Layer Transition and Heat Transfer at Supersonic Speeds. NACA TN 3653, 1956.

9. Van Driest, E. R.: Investigation of Laminar Boundary Layer in Compressible Fluids Using the Crocco Method. NACA TN 2597, 1952.

10. Van Driest, E. R.: The Turbulent Boundary Layer on a Cone in a Supersonic Flow at Zero Angle of Attack. Rep. AL-1042, Aerophys. Lab., North American Aviation, Inc., Mar. 22, 1951. (Contract W33-038ac-14191, Proj. MX-770.)

11. Cohen, Clarence B., and Reshotko, Eli: The Compressible Laminar Boundary Layer with Heat Transfer and Arbitrary Pressure Gradient. NACA TN 3326, 1955.

[redacted]

12. Van Driest, E. R.: Turbulent Boundary Layer in Compressible Fluids. Jour. Aero. Sci., vol. 18, no. 3, Mar. 1951, pp. 145-161.

13. Rubesin, Morris W.: A Modified Reynolds Analogy for the Compressible Turbulent Boundary Layer on a Flat Plate. NACA TN 2917, 1953.

14. Becker, John V., and Korycinski, Peter F.: Heat Transfer and Pressure Distribution at a Mach Number of 6.8 on Bodies with Conical Flares and Extensive Flow Separation. NACA RM L56F22, 1956.

15. Lees, Lester: The Stability of the Laminar Boundary Layer in a Compressible Fluid. NACA Rep. 876, 1947. (Supersedes NACA TN 1360.)

16. Dunn, D. W., and Lin, C. C.: On the Stability of the Laminar Boundary Layer in a Compressible Fluid. Jour. Aero. Sci., vol. 22, no. 7, July 1955, pp. 455-477.

17. Van Driest, E. R.: Calculation of the Stability of the Laminar Boundary Layer in a Compressible Fluid on a Flat Plate with Heat Transfer. Jour. Aero. Sci., vol. 19, no. 12, Dec. 1952, pp. 801-812.

18. Jack, John R., and Diaconis, N. S.: Variation of Boundary-Layer Transition with Heat Transfer on Two Bodies of Revolution at a Mach Number of 3.12. NACA TN 3562, 1955.

19. Anon.: Free Flight Rocket Material Characteristics. Rep. No. A-10-a, Tech. and Eng. Div., Rocket Div. Branch, Redstone Arsenal, Huntsville (Ala.).

TABLE I. - TWO-STAGE TEST BODY: PHYSICAL DATA

Gross weight at launching (both stages less igniters), lb	235.5
Gross weight of second stage (less igniters), lb	77.0
Gross weight of booster (with coupling assembly), lb	158.5
Coupling assembly weight, lb	3.0
Weight of second stage at burnout, lb	43.3
Telemeter package weight, lb	16.0
Center of gravity at launching[1], in.	76.22
Center of gravity at first-stage burnout[1], in.	61.90
Center of gravity of second stage after separation[1], in.	41.65
Center of gravity of second stage after burnout[1], in.	33.00
Booster fin area (2 fins), sq in.	152.0
Second-stage fin area (2 fins), sq in.	24.2
Included wedge angle, second-stage wedge fin, deg	10
Body diameter, booster, in.	9.32
Body diameter, second stage, in.	6.00
Included cone angle, second stage, deg	15
Skin material, second stage	Inconel
Surface finish of instrumented cone cylinder, microin. rms	~2

[1]From nose tip.

[redacted]

TABLE II. - ROCKETS

[Ref. 19]

Rocket	Gross weight, lb	Propellant weight, lb	Average thrust, lb	Impulse	Gross weight specific impulse	Propellant specific impulse	Burning time, sec
Sustainer (T-55)	45.8	33.5	[a]3900	[a]6,950	[a]152	[a]208	[a]1.60
Booster (T-40)	132.0	103.0	[b]3500	[b]21,000	[b]159	[b]204	5.22

[a]At -20° F and sea level.

[b]At 130° F and sea level.

4263

	Station, in.	Wetted surface distance, in.	Skin thickness, in.	θ
A	3.10	3.38	0.0583	180°
B	6.54	6.84	.0574	$184^{\circ}20'$
C	9.84	10.18	.0570	180°
D	13.25	13.60	.0566	$181^{\circ}14'$
E	16.40	16.77	.0563	$181^{\circ}21'$
F	19.32	19.73	.0561	$177^{\circ}39'$
G	19.40	19.79	.0561	0°
H	21.65	22.07	.0295	$179^{\circ}7'$
I	26.30	26.72	.0290	$182^{\circ}17'$
J	31.72	32.13	.0290	$176^{\circ}13'$
K	60.81	61.23	.0290	$165^{\circ}42'$
L	67.56	67.98	.0272	$128^{\circ}48'$

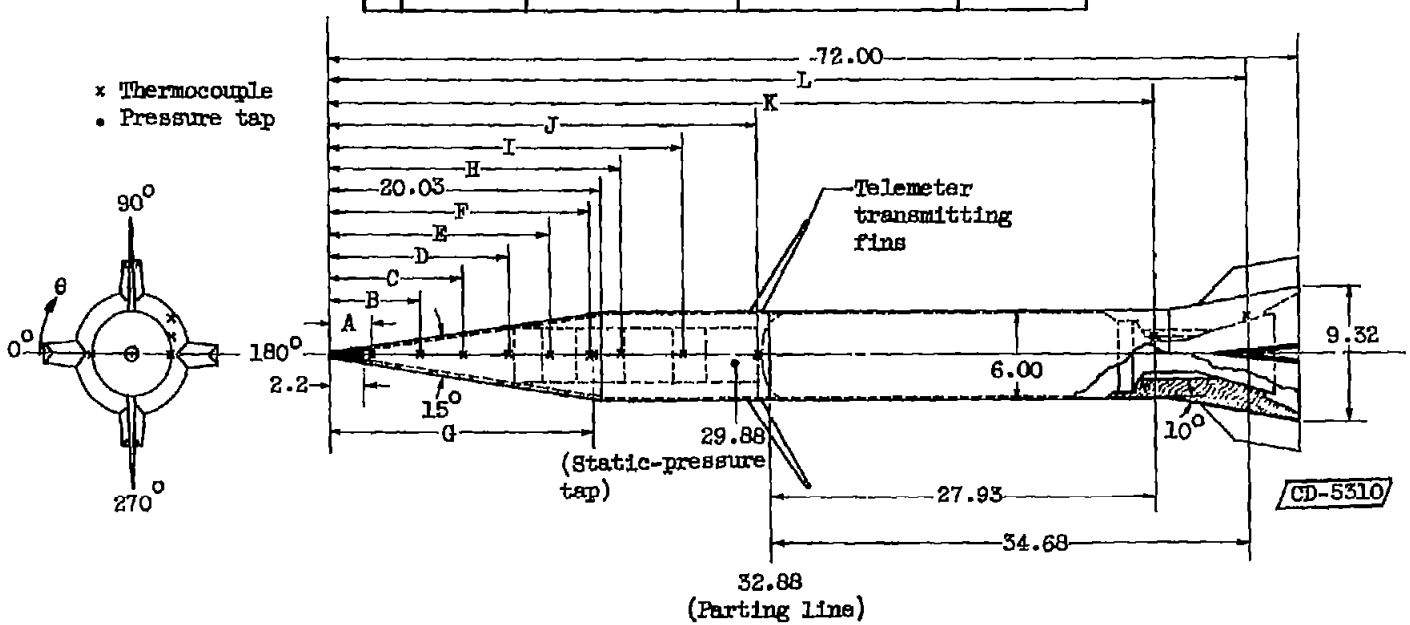

Figure 1. - Sketch of test body showing some physical dimensions and location of thermocouples and pressure tap (dimensions in inches).

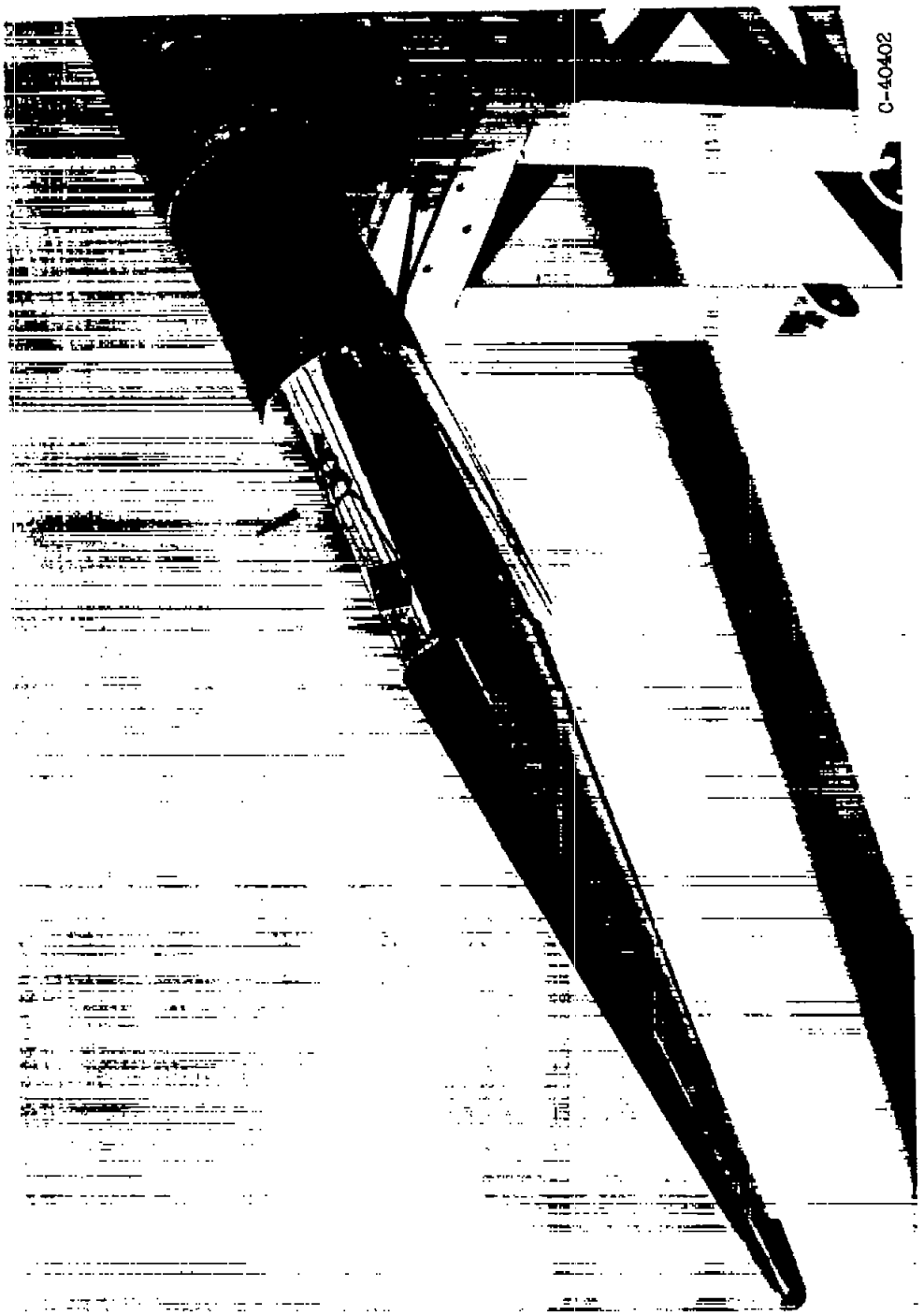

Figure 2. - Highly polished forebody.

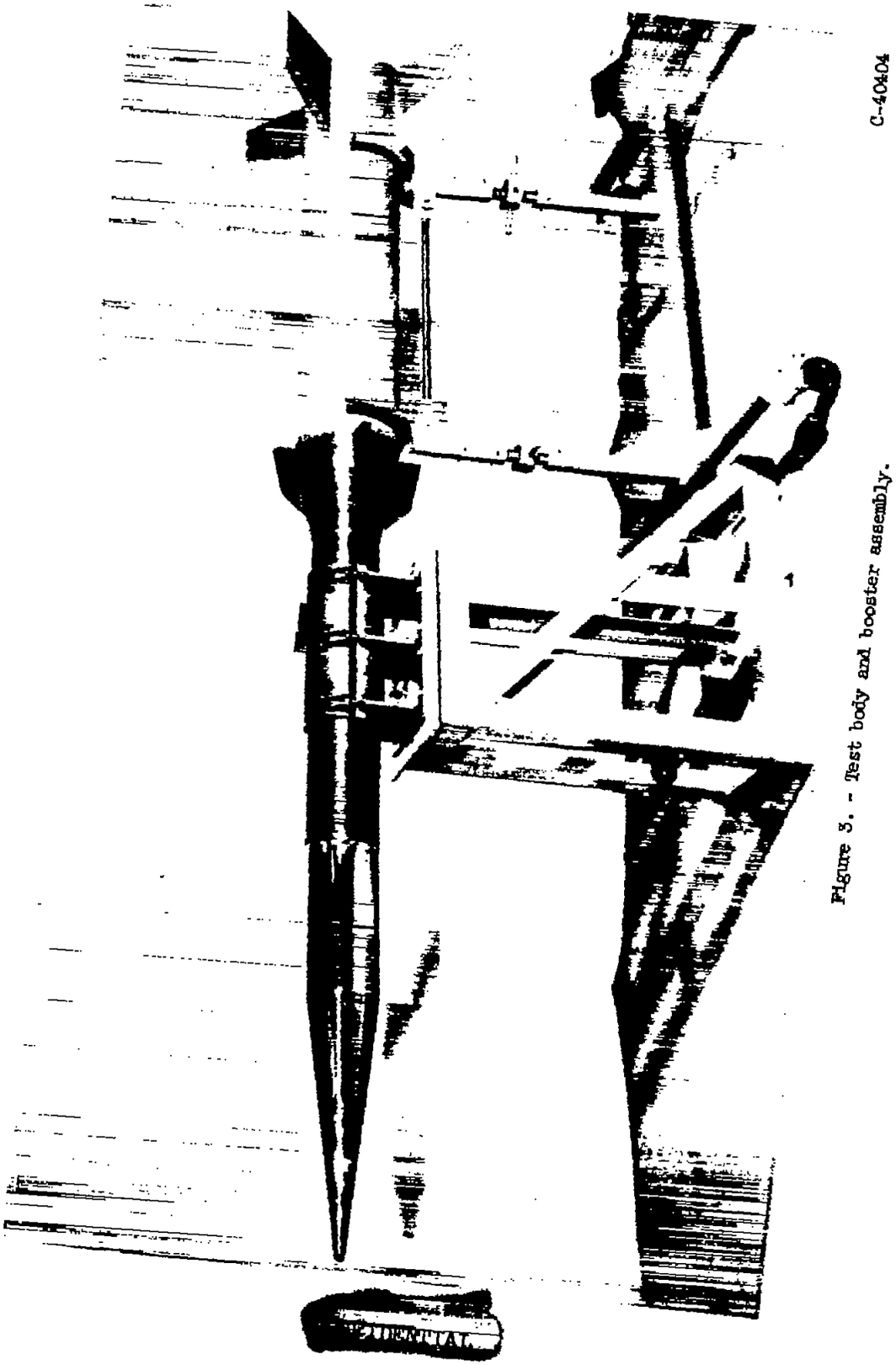

C-40404

Figure 3. - Test body and booster assembly.

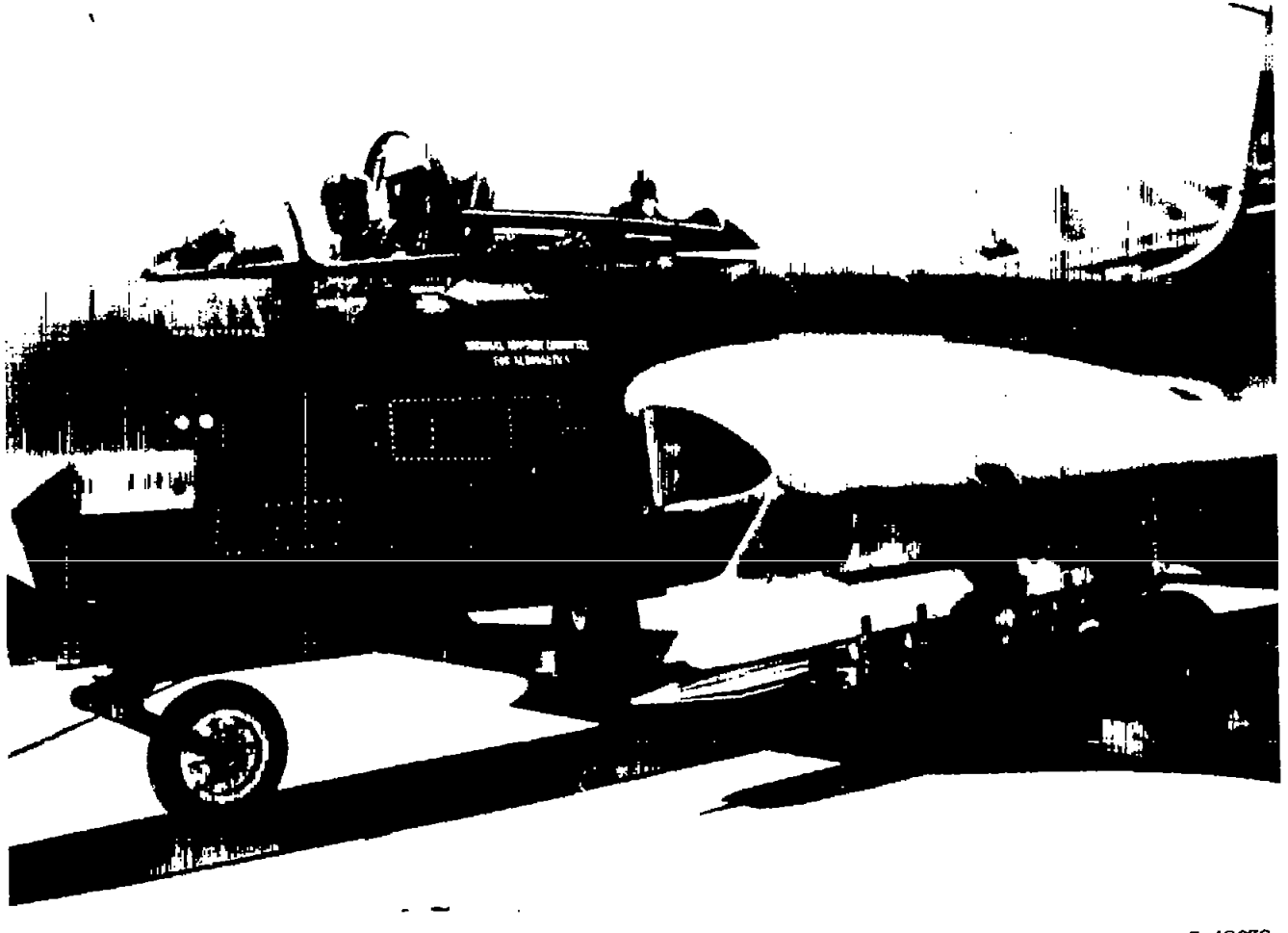

C-42639

Figure 4. - Test body mounted under F2H-2B airplane.

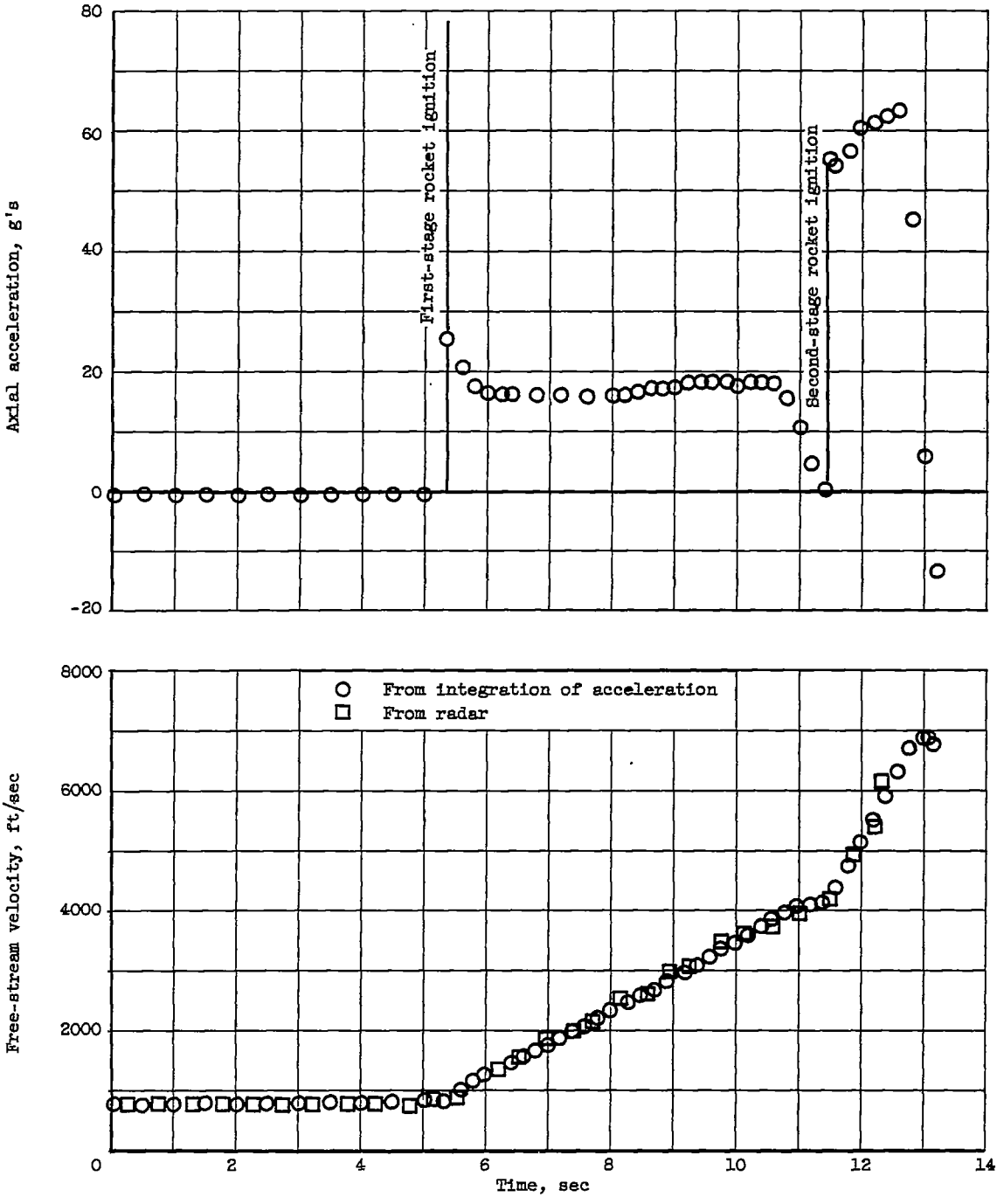

Figure 5. - Variation of axial acceleration and free-stream velocity with time.

[redacted]

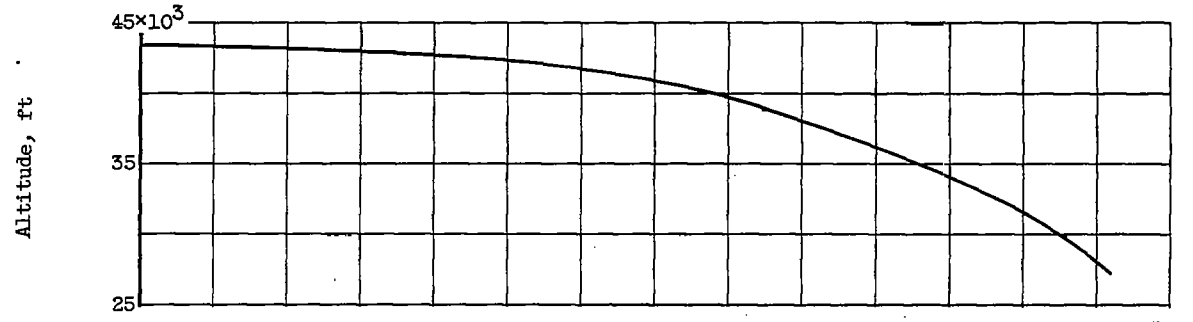

(a) Altitude.

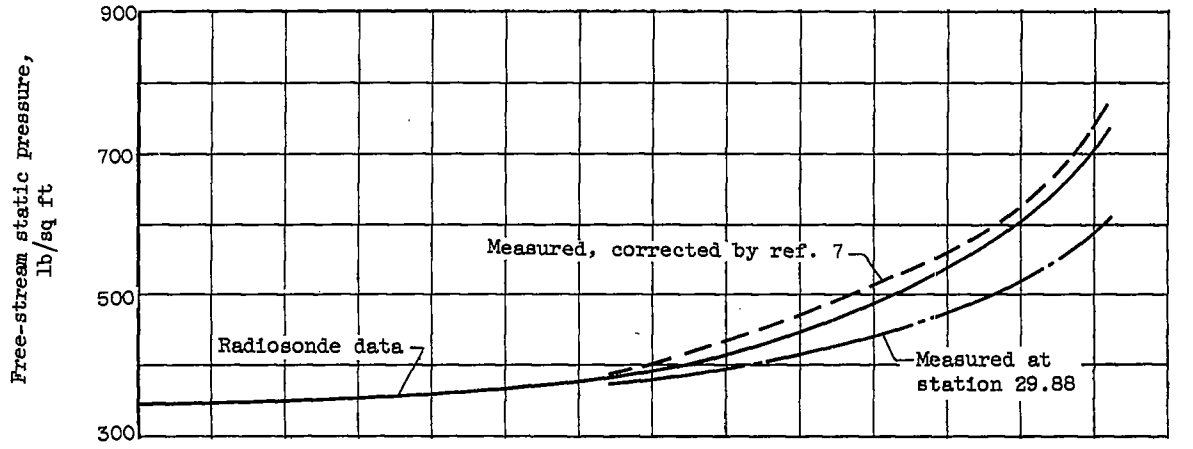

(b) Static pressure.

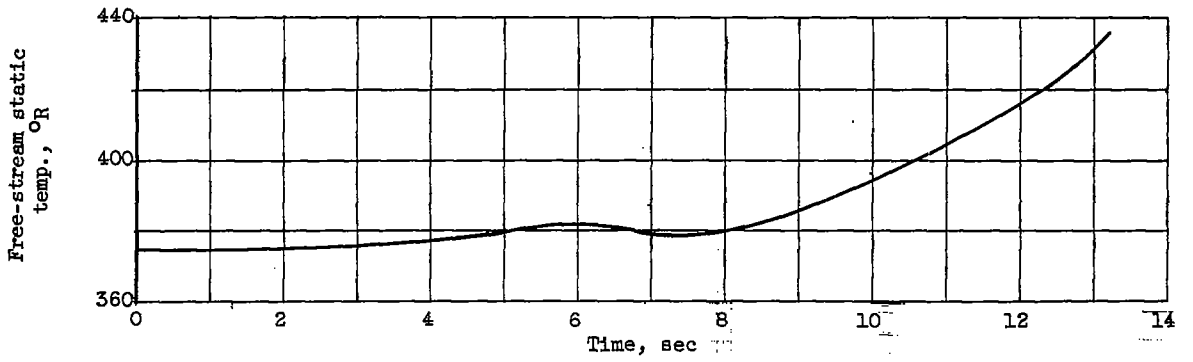

(c) Static temperature.

Figure 6. - Variation of free-stream conditions with time.

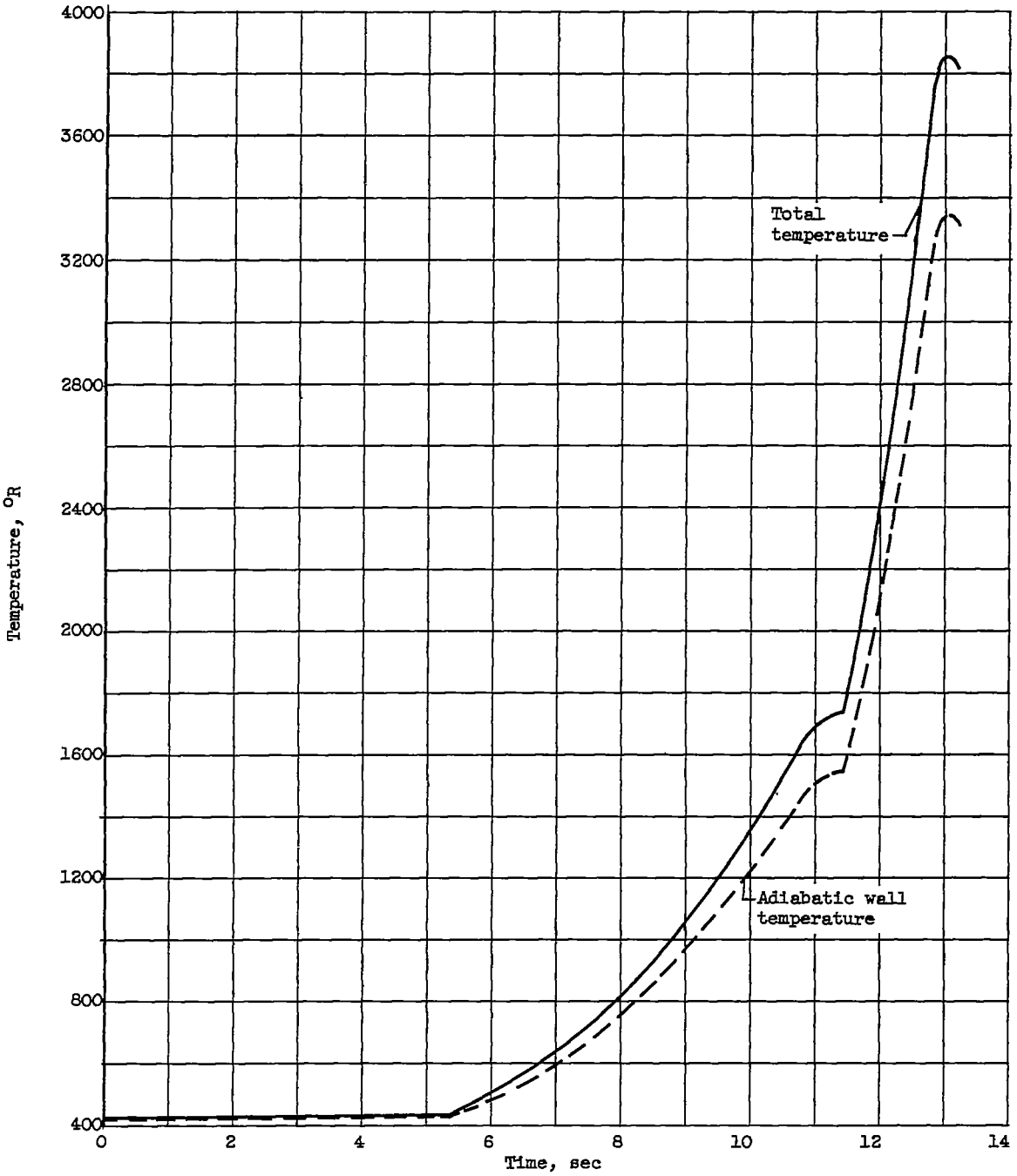

(d) Total temperature and adiabatic wall temperature.

Figure 6. - Continued. Variation of free-stream conditions with time.

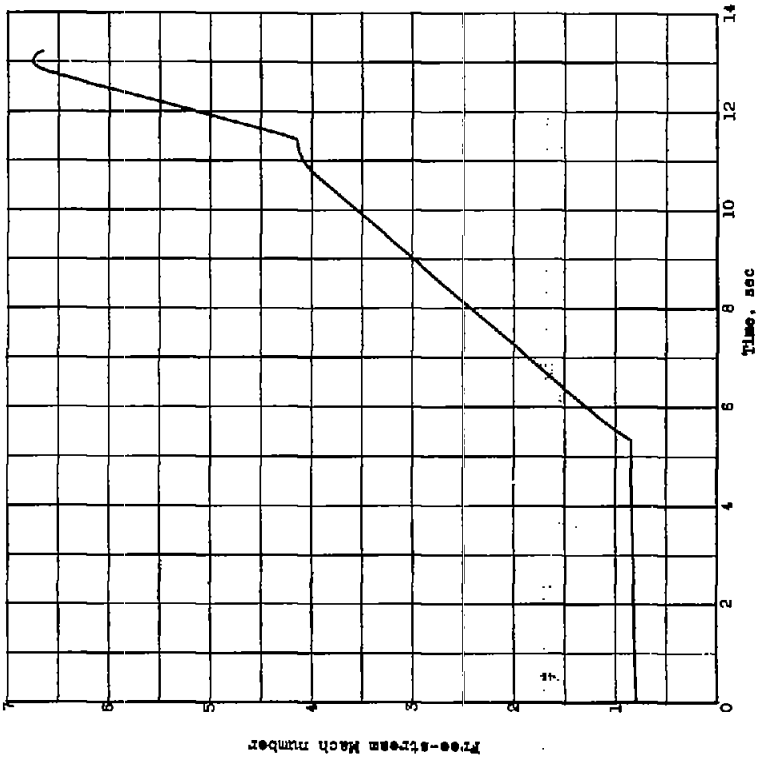

(f) Mach number.

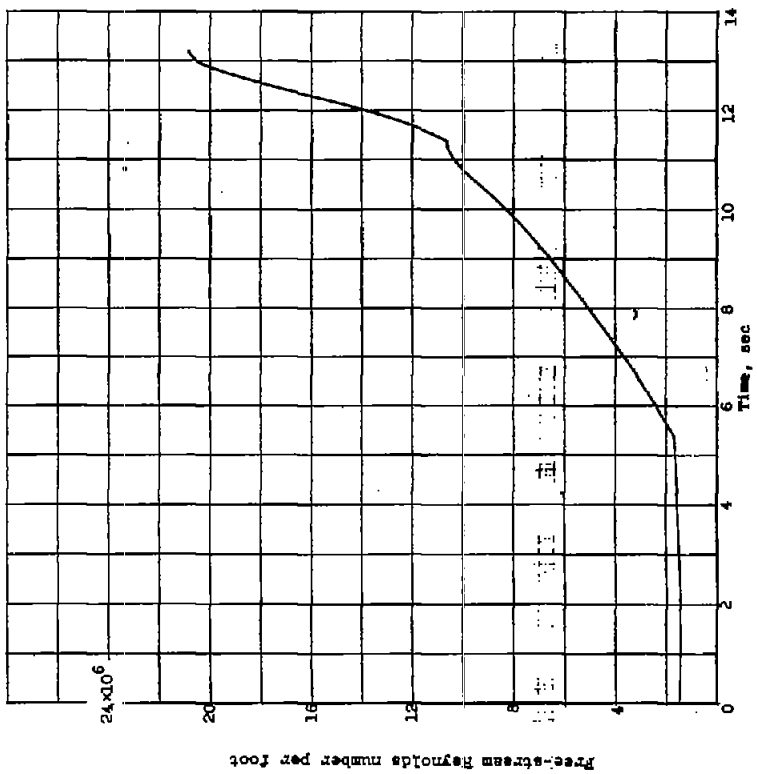

(e) Reynolds number per foot.

Figure 8. - Concluded. Variation of free-stream conditions with time.

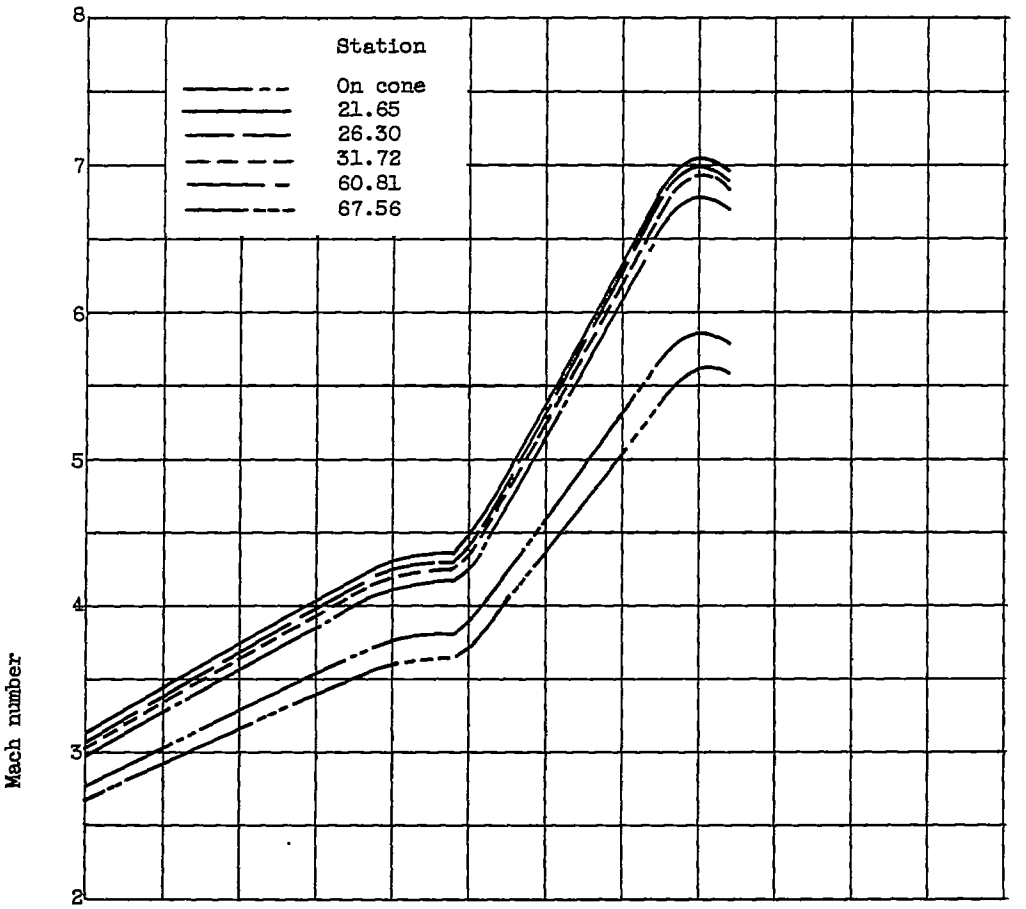

(a) Sharp-tip conditions.

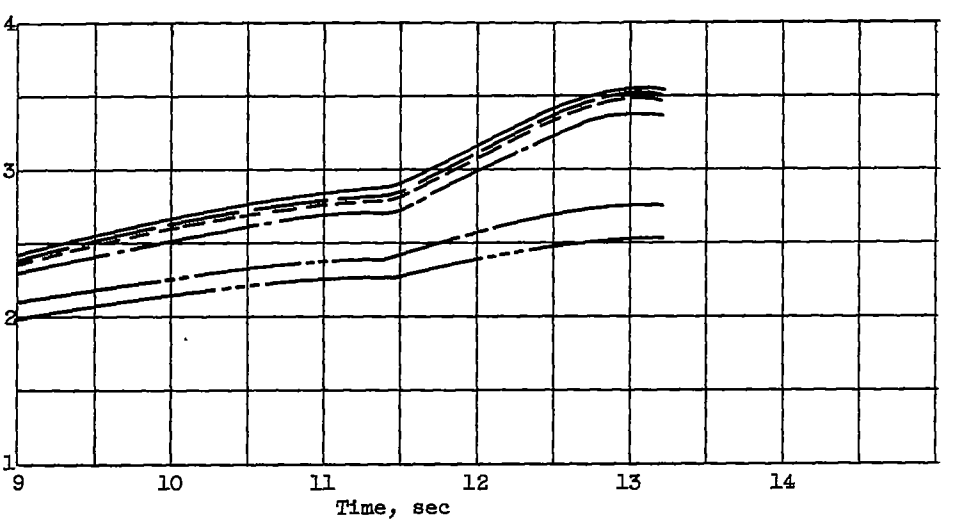

(b) Blunt-tip conditions.

Figure 7. - Variation of Mach number outside boundary layer with time.

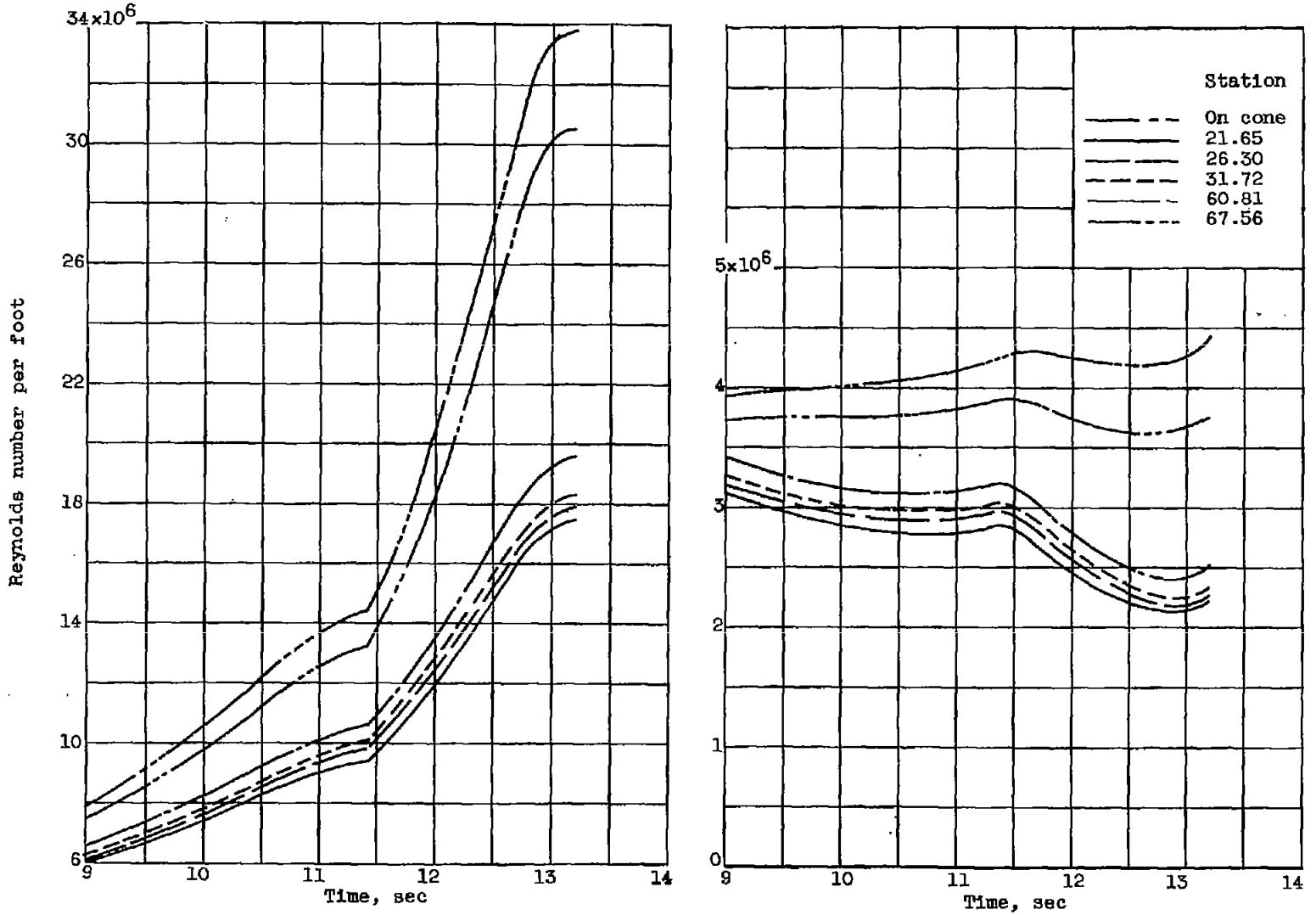

(a) Sharp-tip conditions.

(b) Blunt-tip conditions.

Figure 8. - Variation of Reynolds number per foot outside boundary layer with time.

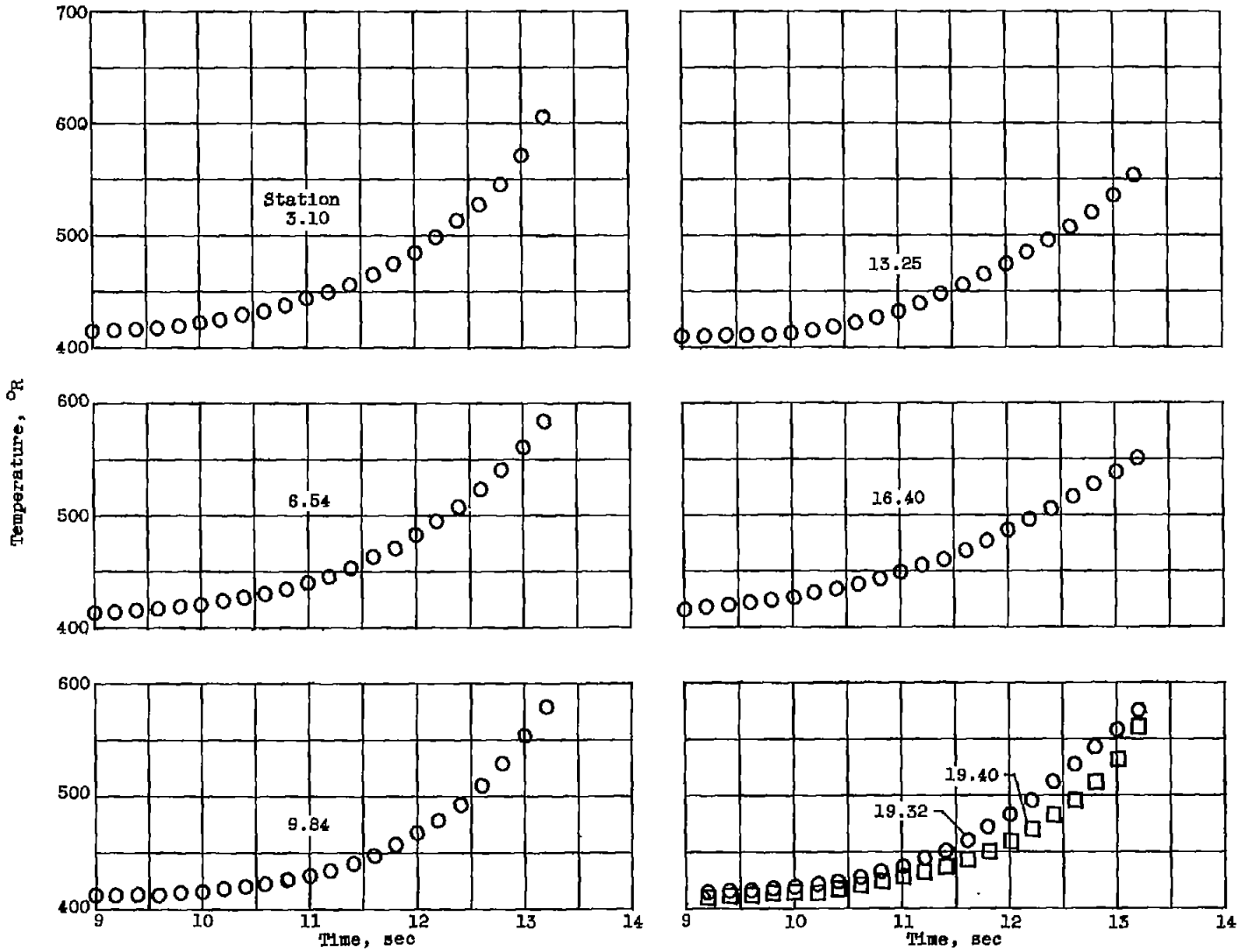

(a) Stations 3.10, 6.54, and 9.84.

(b) Stations 13.25, 16.40, and 19.32 and 19.40.

Figure 9. - Variation of skin temperatures with time.

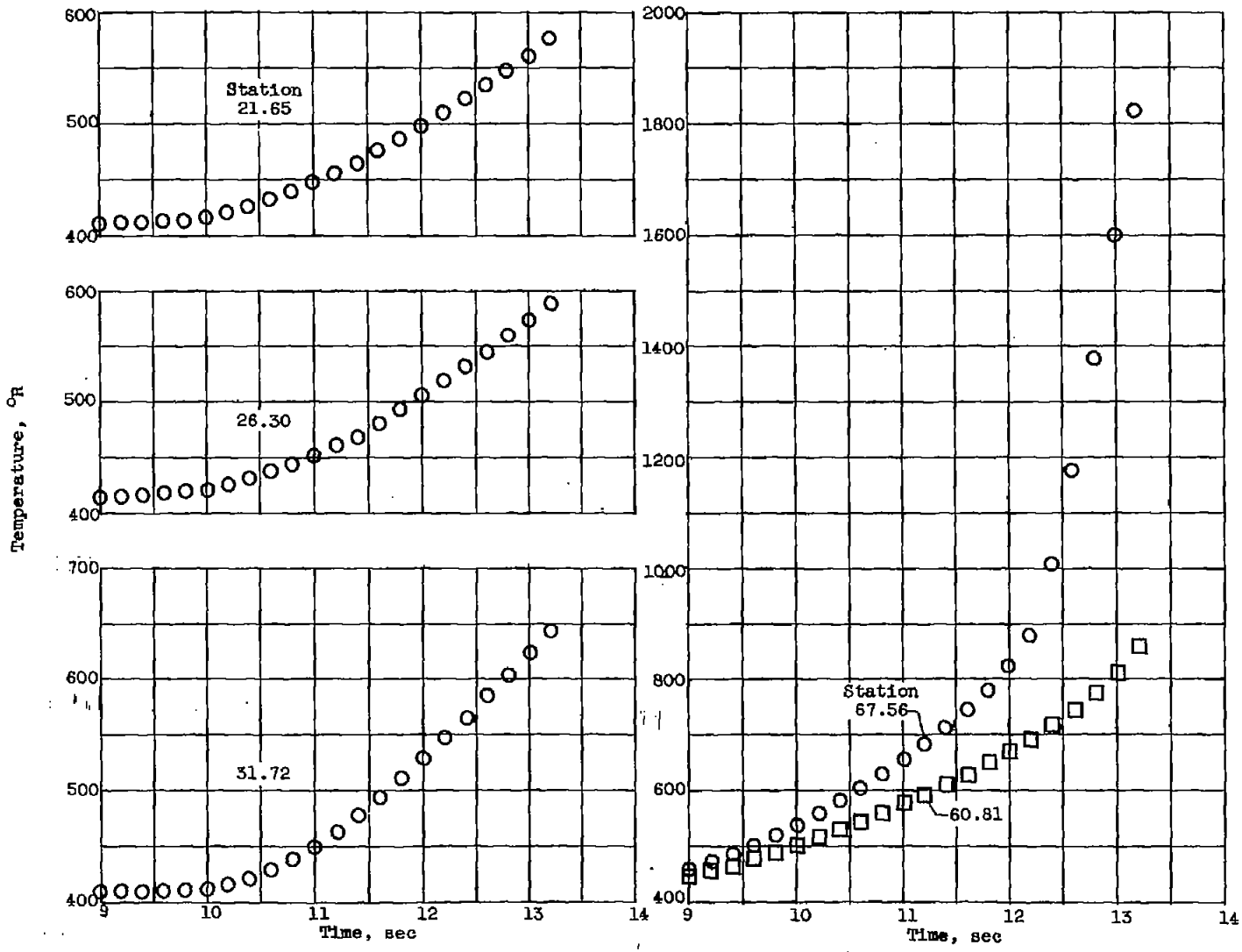

(c) Stations 21.65, 26.30, and 31.72.

(d) Stations 60.81 and 67.56

Figure 9. - Concluded. Variation of skin temperatures with time.

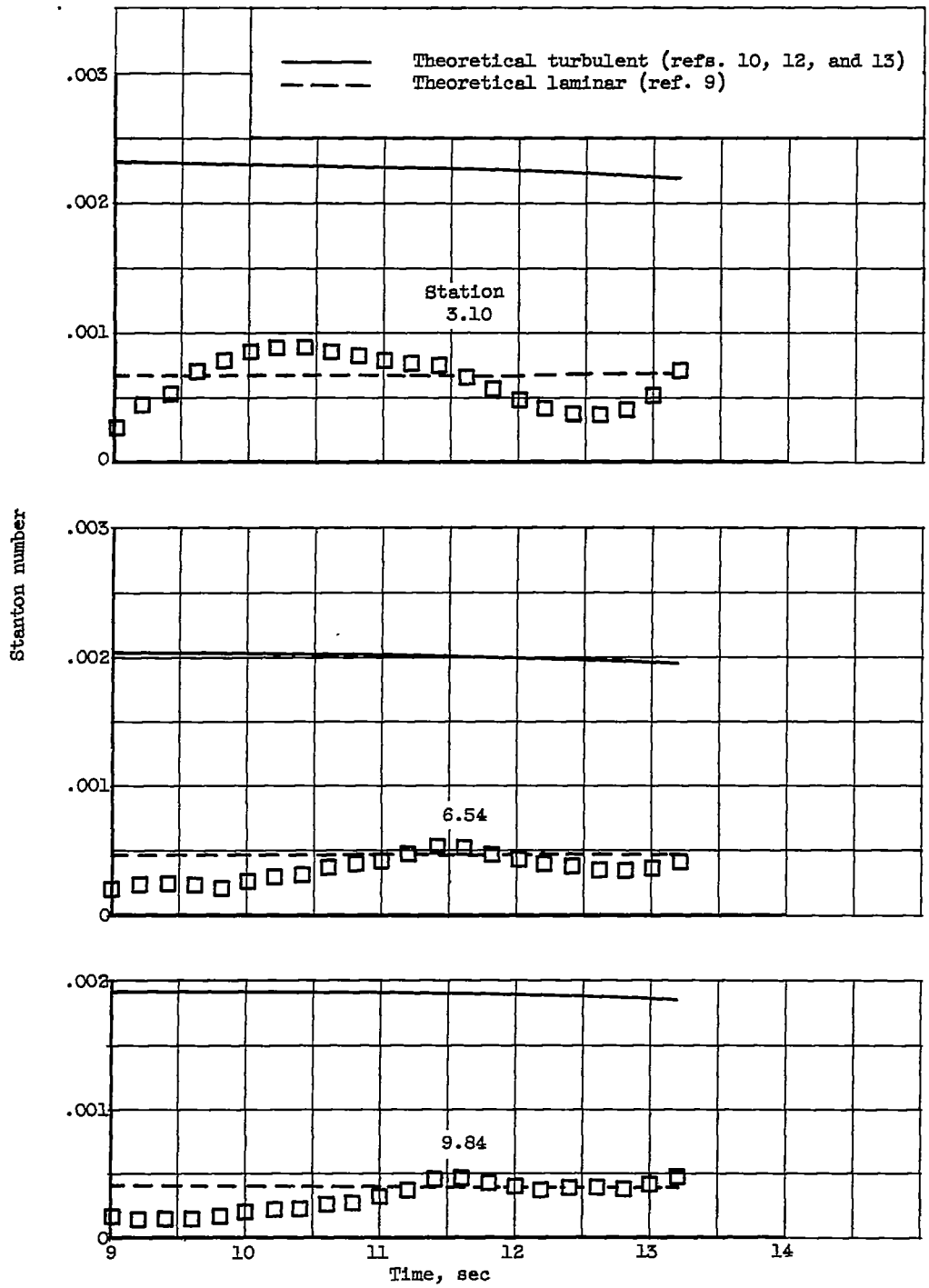

(a) Stations 3.10, 6.54, and 9.84.

Figure 10. - Comparison of local Stanton number with laminar and turbulent theory (blunt-tip conditions).

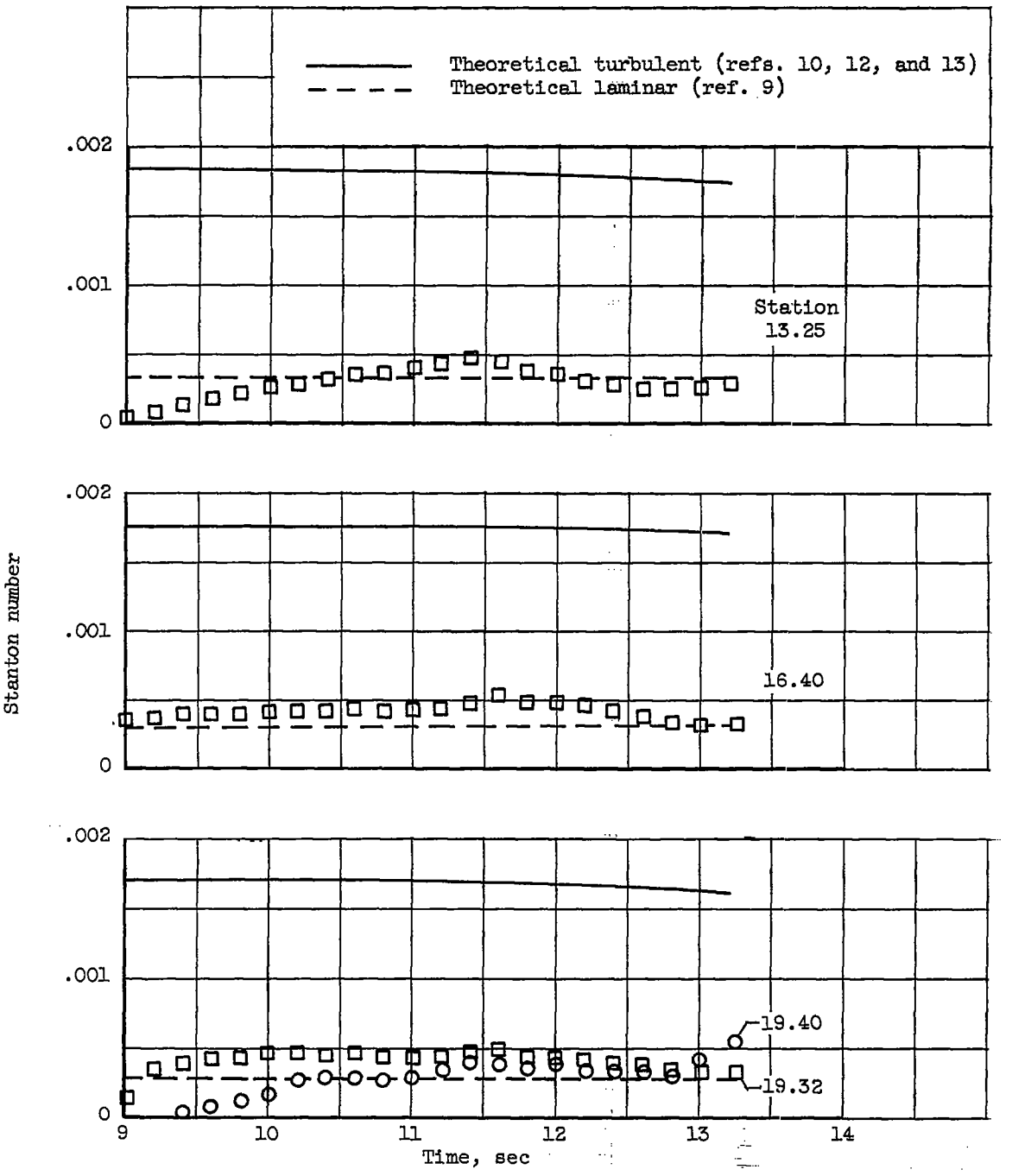

(b) Stations 13.25, 16.40, 19.32, and 19.40.

Figure 10. - Continued. Comparison of local Stanton number with laminar and turbulent theory (blunt-tip conditions).

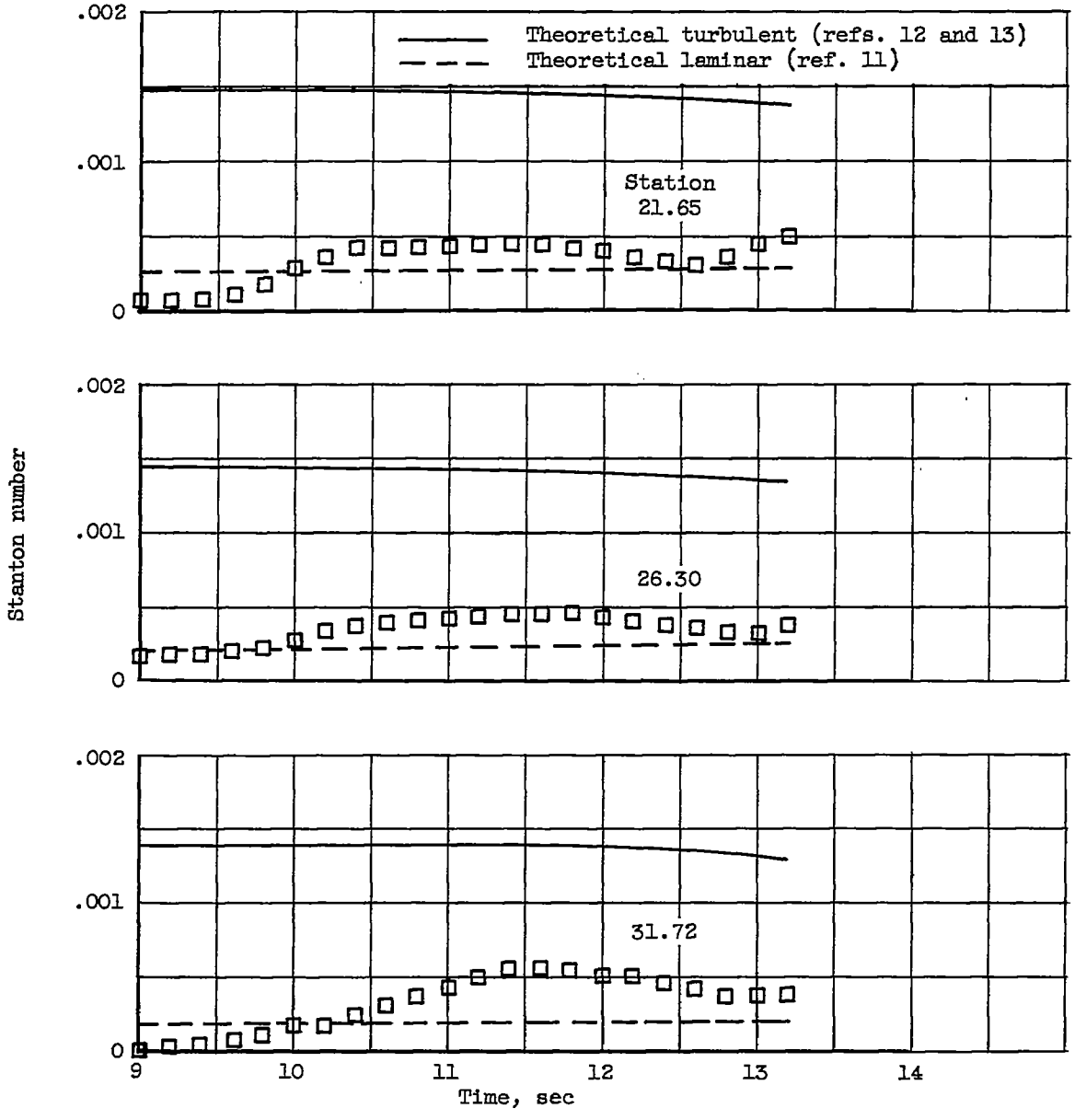

(c) Stations 21.65, 26.30, and 31.72.

Figure 10. - Continued. Comparison of local Stanton number with laminar and turbulent theory (blunt-tip conditions).

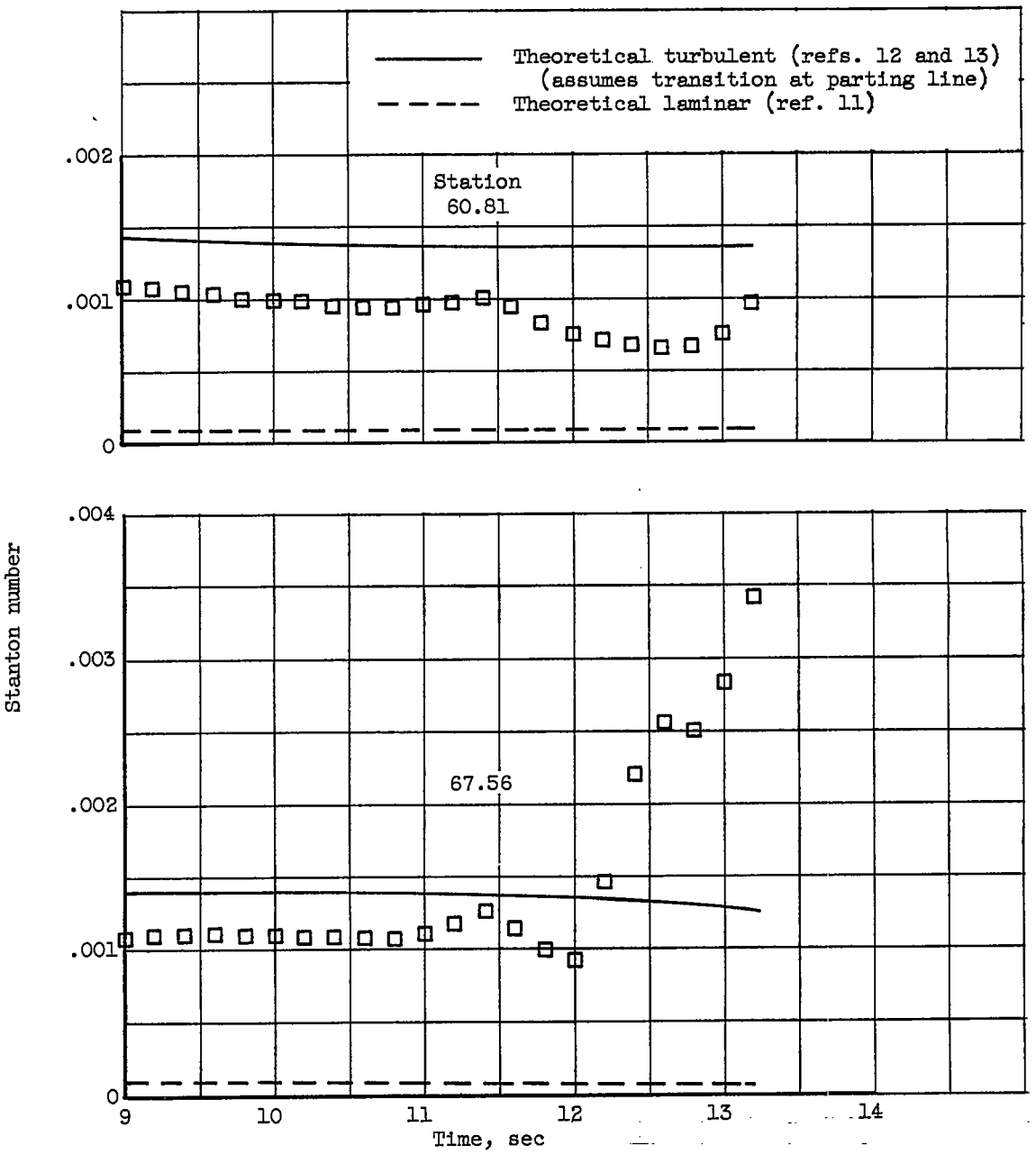

(d) Stations 60.81 and 67.56.

Figure 10. - Concluded. Comparison of local Stanton number with laminar and turbulent theory (blunt-tip conditions).

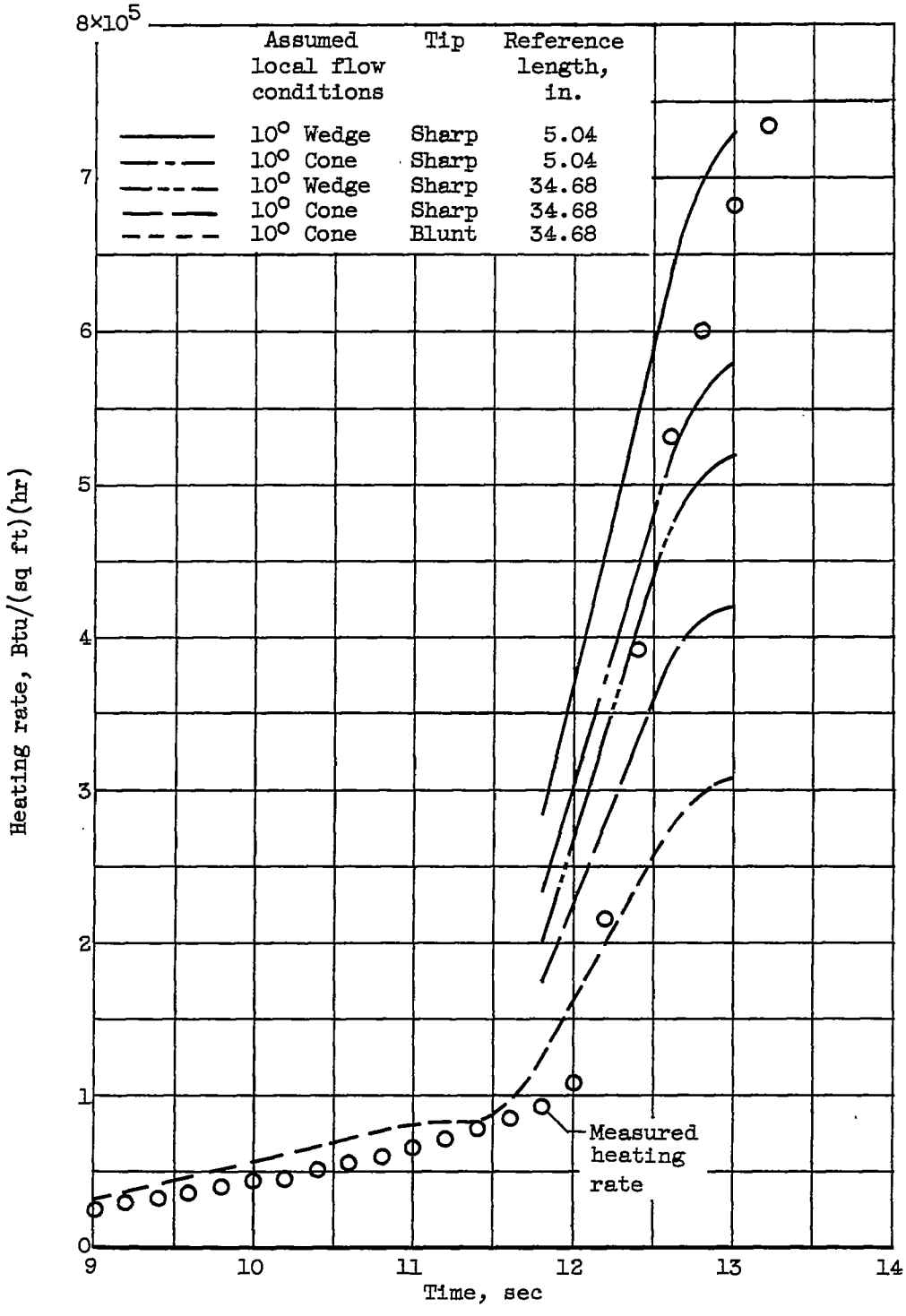

Figure 11. - Heating rate at station 67.56.

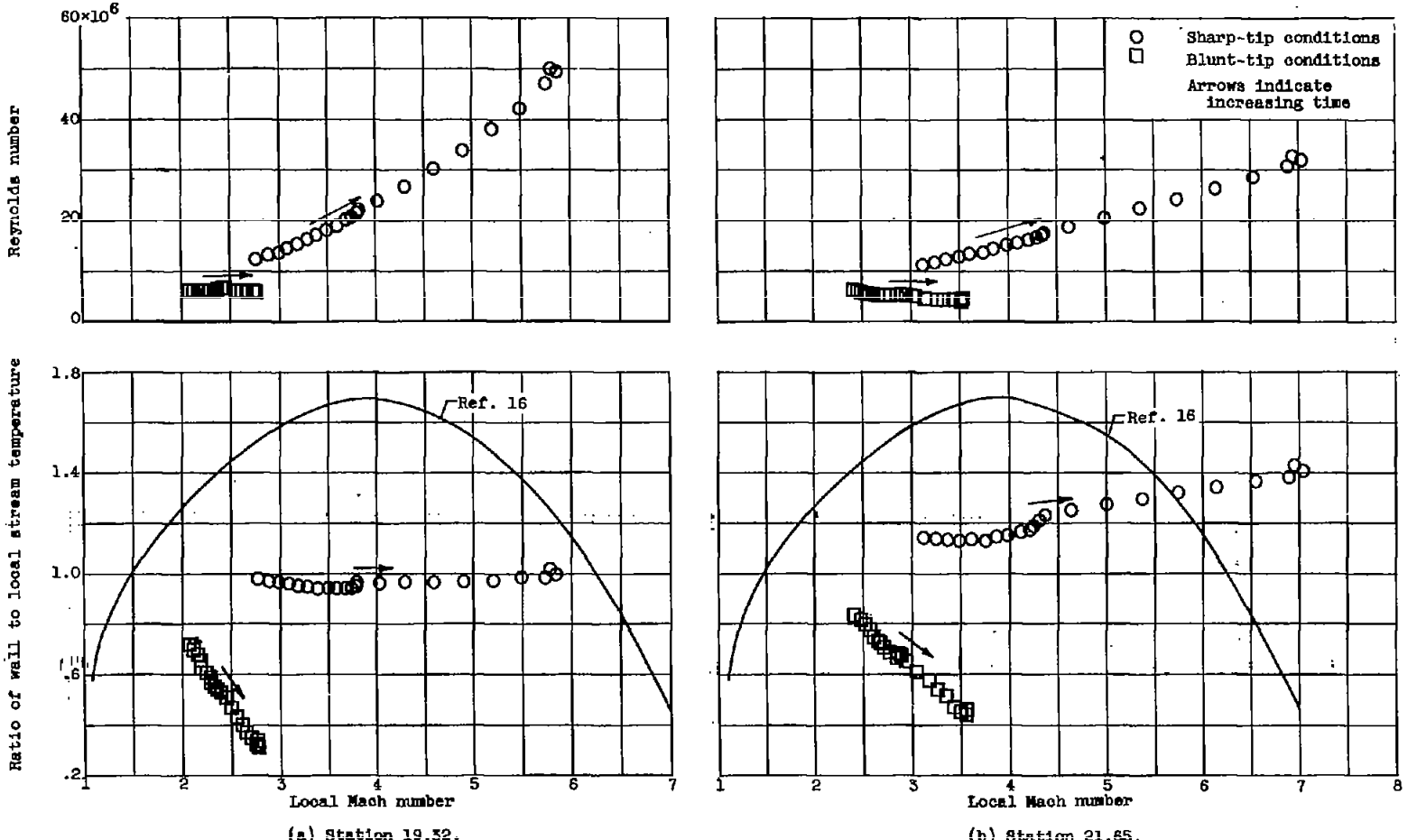

(a) Station 19.32.

(b) Station 21.85.

Figure 12. - Variation of Reynolds number and ratio of wall to local stream temperature with local Mach number.

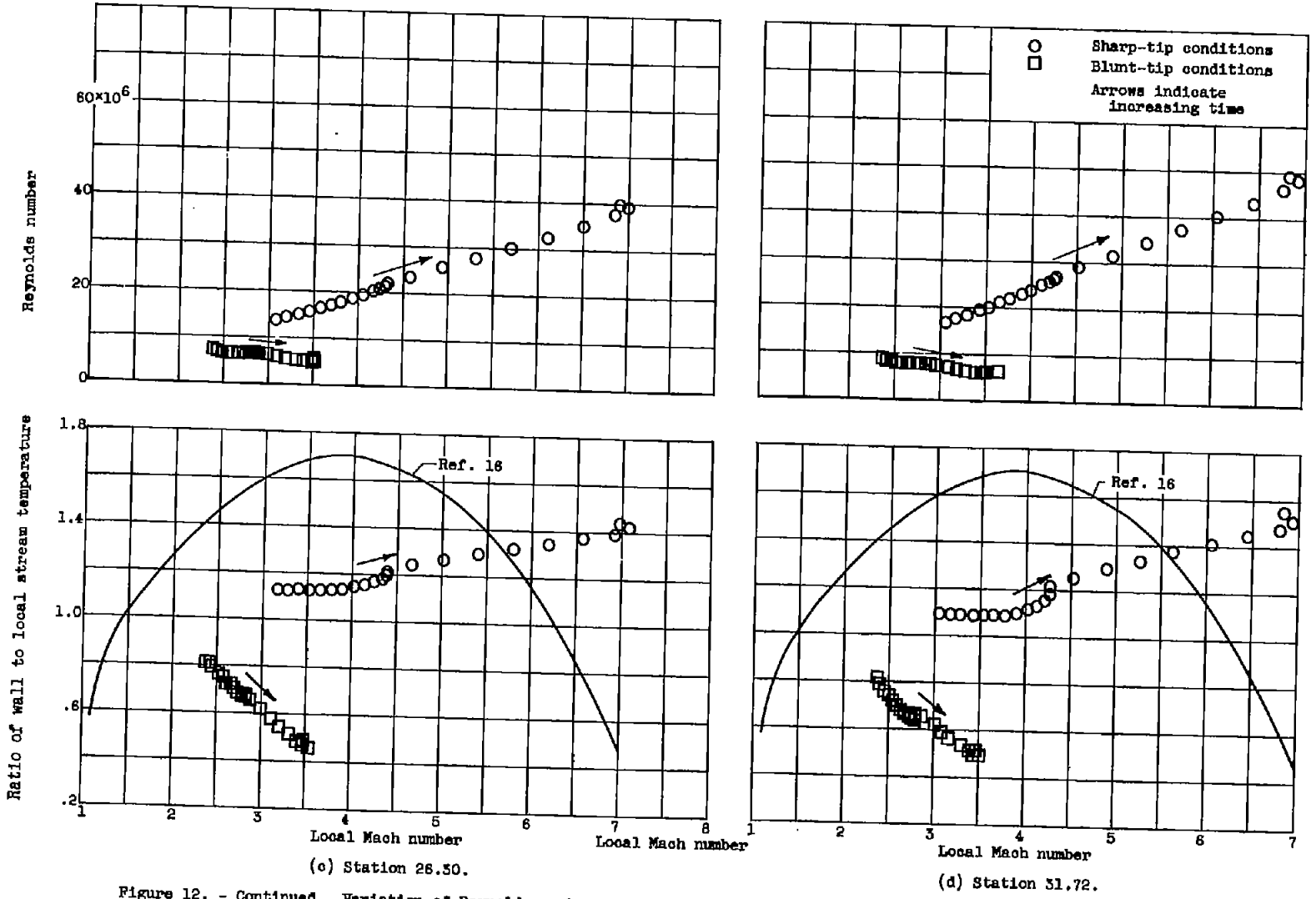

(c) Station 28.50.

(d) Station 31.72.

Figure 12. - Continued. Variation of Reynolds number and ratio of wall to local stream temperature with local Mach number.

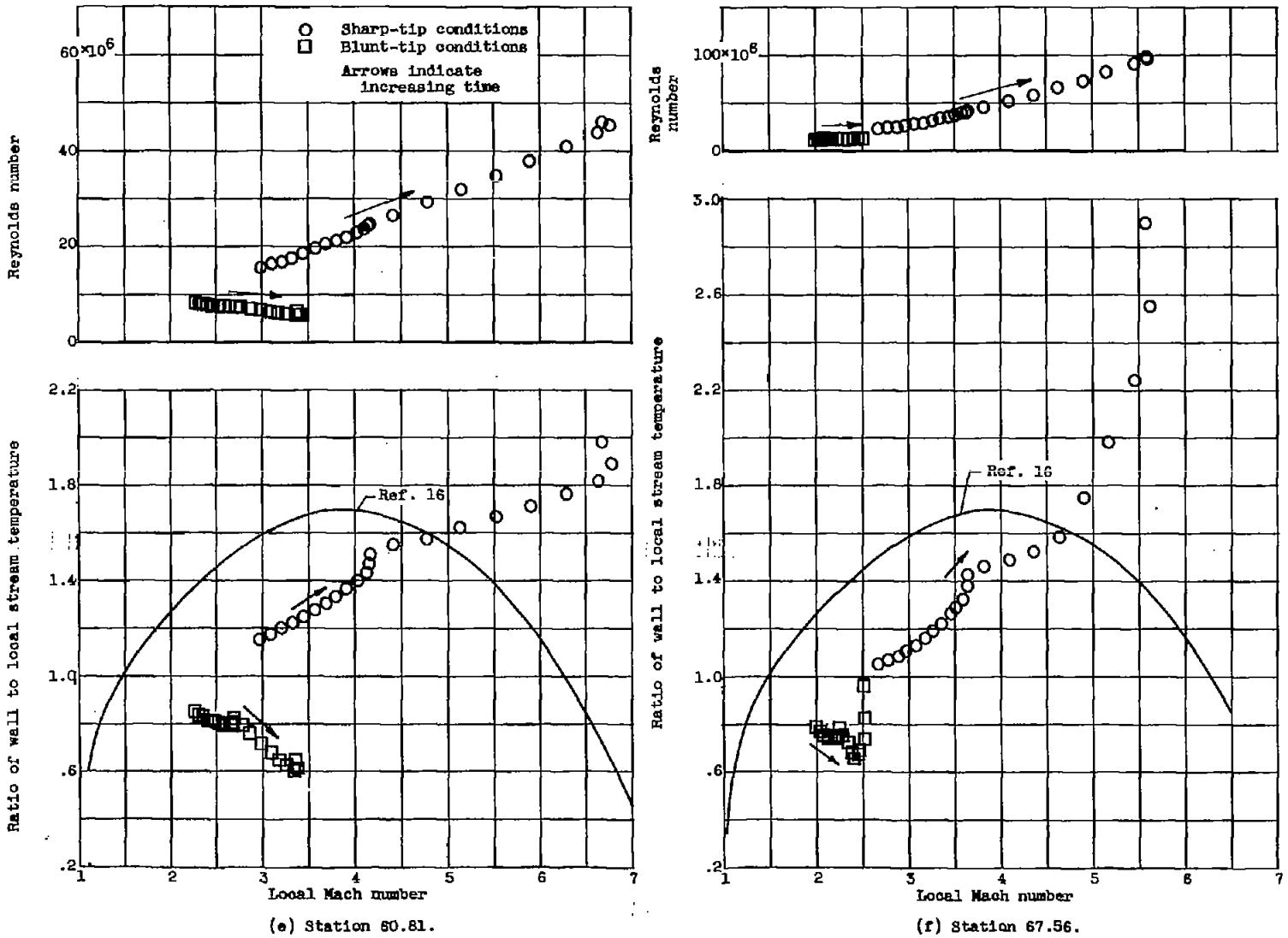

(e) Station 60.81.

(f) Station 67.56.

Figure 12. - Concluded. Variation of Reynolds number and ratio of wall to local stream temperature with local Mach number.

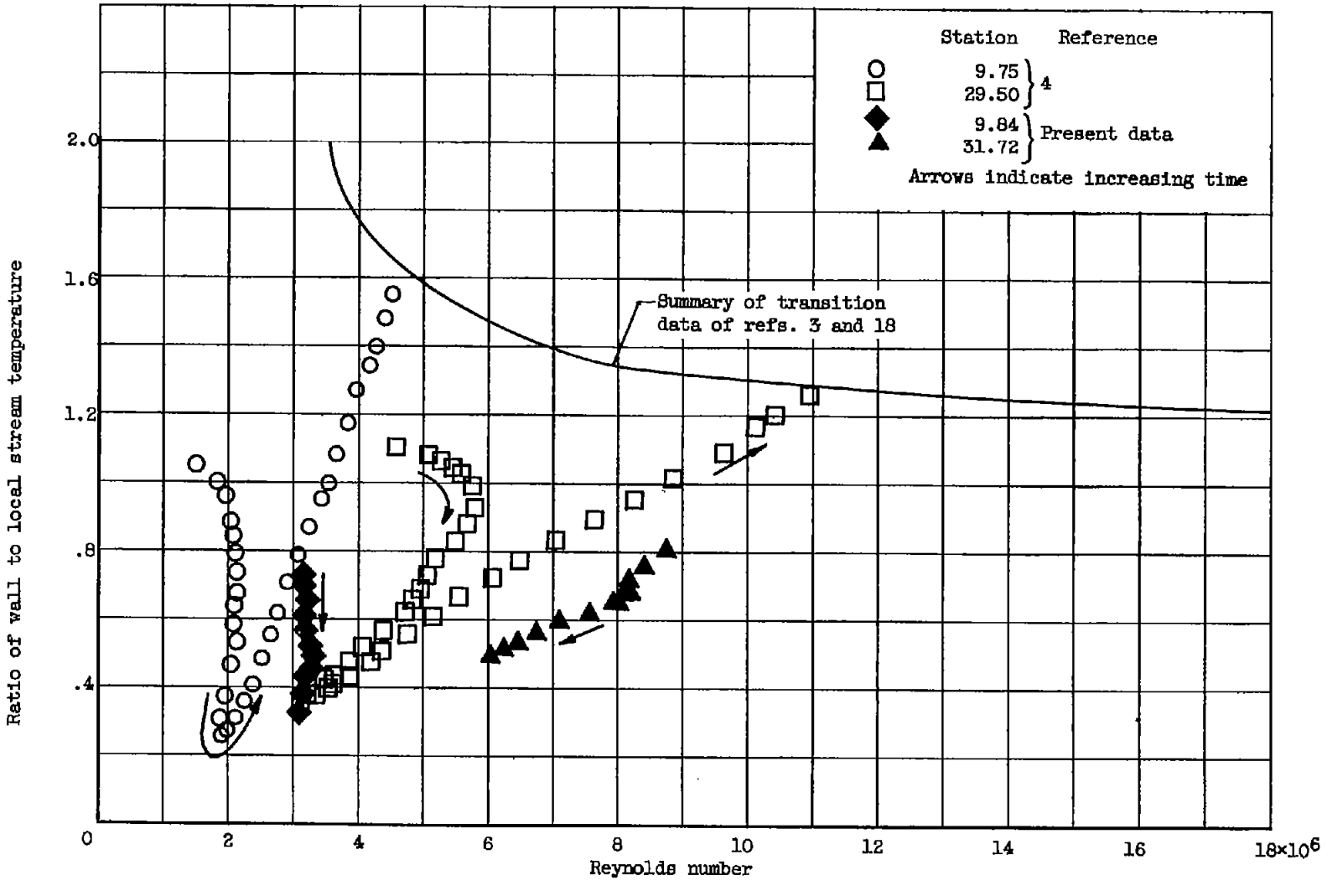

Figure 13. - Comparison of Reynolds numbers and ratios of wall to local stream temperature with previously obtained data. Blunt-tip conditions.